A Waveform-Based Power Estimator For Variable Power Loads

Warit Wichakool, Zachary Remscrim, Uzoma A. Orji, Dr. Steven B. Leeb

Department of Electrical Engineering and Computer Sciences
Massachusetts Institute of Technology
Cambridge, MA, USA
E-mail: sbleeb@mit.edu

***Abstract*—This paper proposes a method to derive an estimator that predicts the power consumption of variable power loads from a subset of higher current harmonics without requiring a full analysis of the internal circuit of the load. The method exploits structural features of the current waveforms consumed by the load to develop the estimator. The computation involves Gaussian elimination of a cyclotomic field representation to compute the estimator coefficients, avoiding floating-point computational error. Experimental results have shown that the proposed algorithm can derive estimators that can extract the power consumption of variable speed drives, computers, or light dimmers from fixed power loads in aggregate measurements.**

I. Introduction

This paper introduces a new method for estimating the real and reactive power consumed by a continuously variable load such as a variable speed drive (VSD) operating in a collection of electrical loads. This method estimates the power consumption of the variable load given only aggregate measurements of current. The algorithm exploits structural features of the non-sinusoidal current waveform consumed by many variable power loads. The proposed method is distinct in requiring no internal circuit model or description of the variable load to derive the estimator.

A nonintrusive load monitoring (NILM) system is a "smart" metering device designed to disaggregate the power consumption of each load from aggregate electrical measurements. Each load is identified by real and reactive power consumption and its current harmonics during a start-up transient and steady-state operation [1]–[5]. The pattern recognition algorithm used in the NILM exploits the fact that many loads such as lights and motors consume approximately discrete power levels. A NILM with a transient event detector can recognize turn-on and turn-off events and track energy consumption.

The application of power electronics enables many loads to operate over a wide variable power range. Examples of variable power loads are variable speed drives (VSDs), computers, and light dimmers. These continuously variable power loads do not have a unique power consumption pattern. Therefore, these loads cannot necessarily be tracked for energy consumption strictly by examining turn-on and turn-off transients. These loads, e.g. a VSD, may consume harmonic currents such as the fifth and seventh harmonics. At a particular site, these harmonics may be uniquely associated with the VSD and can be used to estimate the fundamental current harmonic and the power consumption of the VSD accurately using a data-driven model [6]. The estimating function based on empirical data is sensitive to changes in the environment such as input voltage harmonics [7]. An alternative estimator was developed by modeling and analyzing the behavior of the internal circuit of the VSD, specifically the uncontrolled three-phase rectifier [7]. The model-based estimator solves the issue of the input voltage distortions, enhancing the robustness of the estimator. However, other loads may be too complex to model and analyze. Therefore, the application of the model-based estimator for other variable power loads may not be possible.

Although these variable power loads consume different harmonic currents, there are common characteristics in the current among these loads. These variable power loads are not linear time invariant (LTI) because their currents are modulated by operations of power electronics. As a result, their currents are non-sinusoidal. However, the current waveforms of these variable power loads consist of structural features that can be identified in both the time and frequency domains. For example, the current waveforms of VSDs and computers have known regions of zero current. Furthermore, the sampled current signal is also band-limited and periodic. These observable characteristics of the current waveforms can be used to write linear constraints according to the Fourier analysis and synthesis equations. These constraints can be manipulated using a standard Gaussian elimination method to achieve a functional relationship between the fundamental current harmonic and higher harmonics uniquely associated with the load. The estimator can be computed without fully analyzing the underlying circuit of the load. In addition, the actual computation can be done using a cyclotomic field representation to minimize numerical error [8]–[11].

This paper describes a systematic process to derive a waveform-based estimator. The first section describes the waveform features and their connections to the Fourier analysis and synthesis equations. The next section explains a four-step process to compute the estimator for a particular

This work is supported in part by the ONR's ESRDC program, the Grainger Foundation, and the BP-MIT Research Alliance.

978-1-4577-0541-0/11/$26.00 ©2011 IEEE

load. Finally, the paper includes experimental results demonstrating the capability of the waveform-based estimator to disaggregate the power consumption of continuously variable power loads such as VSDs, computers, and light dimmers from fixed power loads.

II. Background

Instead of fully analyzing the circuit diagram for each new load to compute the estimator, the current waveforms of variable power loads contain information that can be used to distinguish the load from other loads. Current waveforms and discrete Fourier transform (DFT) coefficients of a VSD are shown in Fig. 1. Current waveforms of a computer and a light dimmer are shown in Figs. 2, and 3 respectively. Although the internal circuits of these three loads are different, their current waveforms share a few common properties that can be observed. Those properties include five waveform features:

- periodicity,
- presence of zero-current regions,
- waveform symmetry,
- approximately band-limited signal, and
- real-valued signal.

These five descriptive constraints can be translated to mathematical forms using the Fourier analysis and synthesis equations.

Given a band-limited and periodic signal, the sampled waveform can be described by a weighted sum of discrete Fourier transform (DFT) coefficients I_k as

$$i[n] = \sum_{k=0}^{N-1} I_k e^{j\frac{2\pi}{N}(kn)}, \tag{1}$$

where the variable n is the time index, ranging from 0 to $N-1$. The number N represents a number of samples per signal period. The DFT coefficients I_k are calculated by the Fourier analysis equation,

$$I_k = \frac{1}{N} \sum_{n=0}^{N-1} i[n] e^{-j\frac{2\pi}{N}(kn)}, \tag{2}$$

where the subscript k represents the harmonic, ranging from 0 to $N-1$ [12]. The scaling factor $\frac{1}{N}$ normalizes the coefficients by the data length. The relationship in (1) illustrates the form of the functional relationship among different harmonics and the time-domain waveform.

If all N samples of the current waveform are known, the Fourier synthesis equation (1) provides all constraints between different harmonic currents I_k and the time-domain signal $i[n]$. However, only a limited number of equations can be used to compute the estimator. The next section explains the systematic procedure to translate the five waveform features into the mathematical constraints that can be manipulated into the desired estimator.

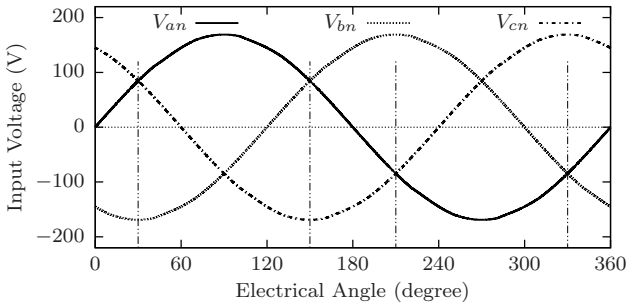

(a) Line voltages

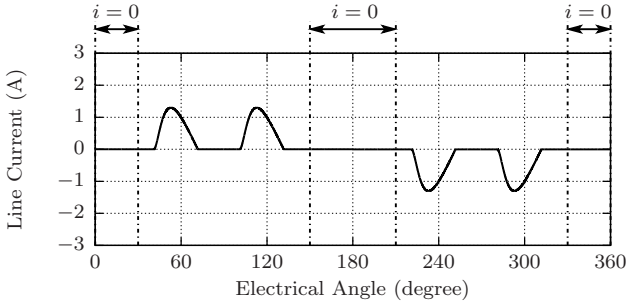

(b)

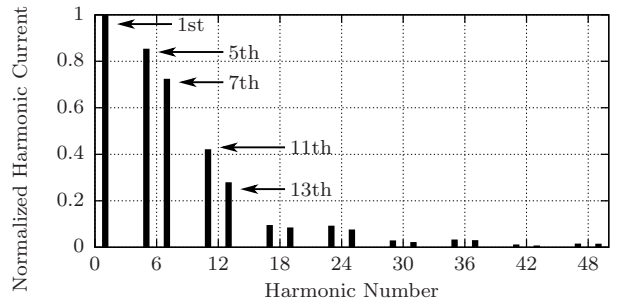

(c)

Fig. 1. Simulated voltage and current waveforms and current harmonics associated with a VSD. Three-phase voltages are shown in (a). The VSD line current for one cycle is shown in (b). The normalized harmonic currents is shown in (c).

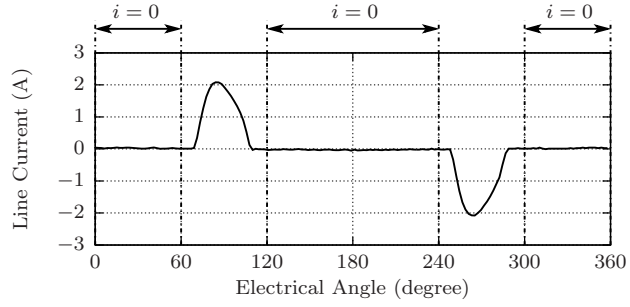

Fig. 2. Experimental current waveform of a computer

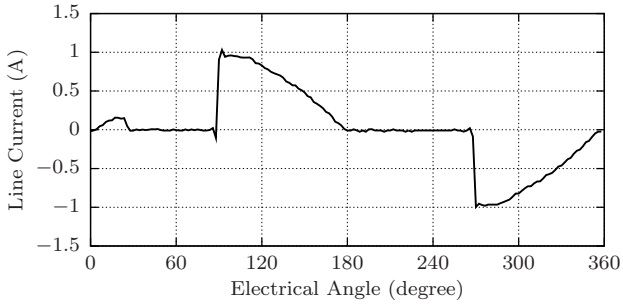

Fig. 3. Experimental current waveform of a light dimmer

III. Estimator Derivation

The goal of the proposed method is to compute a functional relationship between the fundamental harmonic, I_1 and higher harmonics that are uniquely or largely associated with a variable power load at a target site. Specifically, this proposed method is looking for an estimating function in a linear form,

$$\widehat{I_1} = \sum_{m=1}^{2K} (c_m I_m), \tag{3}$$

where $\widehat{I_1}$ is the estimated fundamental harmonic, and the coefficient c_m represents a complex coefficient. The variable I_m represents selected higher harmonics or input harmonics uniquely associated with the variable power load. The number $2K$ represents the number of input harmonics used in the estimator.

The estimator can be developed iteratively with a four-step process:

1) identify signal constraints,
2) setup a Fourier matrix equation,
3) solve for the estimator, and
4) evaluate estimation error.

The first step describes how to translate the five waveform features to linear constraints described in the Fourier synthesis equation (1). This step also includes the selection of the input harmonics used in the estimator. The second step establishes a matrix equation from the constraints. The third step demonstrates how to reduce the matrix equation into the estimator equation. Lastly, the derived estimator is evaluated and tested against accuracy requirements in the fourth step. The procedure can be iterated to further improve the estimation error or to reduce the number of input harmonics.

A. Signal Constraints

First, the current signal in the ac system is assumed to be periodic with a period of T, which is a reciprocal of line voltage frequency. The periodic signal is sampled and analyzed using the discrete Fourier transform to obtain the DFT coefficients or current harmonics I_k according to the Fourier analysis equation (2). The signal is assumed to be sampled at the rate F_s such that the sampled signal consists of N points per period. Given N samples per period, there are N DFT coefficients from the Fourier analysis equation (2).

Second, the current waveform consists of known regions of zero-current because of the circuit operation. In the case of a VSD, the consumed current has known zero-current regions shown in Fig. 1, which can be expressed mathematically based on an electrical angle specified in radians,

$$i[n] = 0 \quad \text{for } \frac{2\pi n}{N} \in \left[0, \frac{\pi}{6}\right] \cup \left[\frac{5\pi}{6}, \frac{7\pi}{6}\right] \cup \left[\frac{11\pi}{6}, 2\pi\right). \tag{4}$$

For a periodic signal $i[n]$ sampled with the rate of N points per period, the first region of zero-current specified in (4) $0 \leq \frac{2\pi n}{N} \leq \frac{\pi}{6}$ can be expressed mathematically using the Fourier synthesis equation (1) as

$$\begin{aligned}
I_0 + I_1 &+ \cdots + I_{N-1} &&= i[0] \\
I_0 + I_1 e^{j\frac{2\pi}{N}} &+ \cdots + I_{N-1} e^{j\frac{2\pi}{N}(N-1)} &&= i[1] \\
I_0 + I_1 e^{j\frac{2\pi}{N}(2)} &+ \cdots + I_{N-1} e^{j\frac{2\pi}{N}(N-1)(2)} &&= i[2] \\
&\vdots &&= \vdots \\
I_0 + I_1 e^{j\frac{2\pi}{N}(N_1)} &+ \cdots + I_{N-1} e^{j\frac{2\pi}{N}(N-1)(N_1)} &&= i[N_1],
\end{aligned} \tag{5}$$

where $\frac{2\pi N_1}{N} = \frac{\pi}{6}$. Similarly, other zero-current regions can also be translated and added to the list of constraints similar to (5) as well.

Third, the load current waveform exhibits a specific symmetry. Load currents shown in Figs. 1, 2, and 3 are approximately odd-symmetric. There are two ways to express this constraint. One method is to express in the time domain as

$$i[n] = -i\left[n + \frac{N}{2}\right], \text{ for } 0 \leq n < \frac{N}{2}. \tag{6}$$

The number $\frac{N}{2}$ indicates the midpoint of the waveform. Alternatively, the constraint can be formulated in the frequency domain as zero even harmonics, specifically

$$I_{k_{\text{even}}} = 0, \tag{7}$$

where the subscript k_{even} represents an even number, including zero. This constraint (7) eliminates all even harmonics from the calculation.

Moreover, a VSD does not consume any triplen harmonic under a balanced three-phase voltage. This constraint can be represented as

$$I_{k_{\text{triplen}}} = 0. \tag{8}$$

Fourth, the current signal is processed through the anti-aliasing filter and the analog-to-digital converter in order to be converted into a digital form properly. The anti-aliasing filter confines the bandwidth of the signal, making the signal approximately band-limited. The histogram of DFT coefficients of a VSD in Fig. 1 shows that most energy of

the current waveform is contained in a low frequency region. The amplitude of higher harmonics are small and can be neglected. The band-limited constraint can be expressed as

$$I_{k_{\text{highfreq}}} = 0 \tag{9}$$

for some $k_{\text{highfreq}} > K_0$, where the parameter K_0 is a user-specified boundary.

Fifth, the real input signal dictates the characteristics of the DFT coefficients, I_k. Given a real signal, the magnitude of the DFT coefficients I_k is even, and the phase the DFT coefficients I_k is odd. In other words, most DFT coefficients are complex conjugate pairs, $I_{N-5} = I_5^*$, for example. The complex conjugate can be used in the selection of the input harmonics.

The estimating function in (3) specifies a subset of DFT coefficients as input harmonics. In this paper, the estimator is derived iteratively as a function of input harmonics, the algorithm must be initialized to a reasonable number of harmonics, i.e. ten, with the goal to reduce this number as low as possible. The iterative process will reduce the number of input harmonics when possible.

The selection of the input harmonics depends on two factors: the availability of the harmonics in the measured signals and the estimation error. In the field, the NILM must observe a collection of harmonics that are uniquely associated with the variable load. With the exception of the fundamental harmonic, other harmonics can be selected as input harmonics in the proposed method. The "input" harmonics should at least correlate with the fundamental harmonic and have non-zero values.

Among the available harmonics, harmonics with larger magnitude should be selected to improve the signal-to-noise ratio (SNR). One selection scheme is to select the input harmonics according to their magnitudes in a descending order. For example, according to the histogram of the current harmonics shown in Fig. 1, the fifth and seventh harmonics are the two largest harmonics among higher harmonics. Therefore, these two harmonics can be selected as the candidates.

The real input signal implies the complex conjugate property of the DFT coefficients. The magnitude of the complex conjugate pair is the same as the harmonic itself. In the actual implementation, not all DFT coefficients have to be computed in real time. Only the input harmonics are necessary in the estimation. The complex conjugate pair requires no additional computation. As a result, the complex conjugate pairs of the candidate input harmonics can be used as the input harmonics with a negligible computational cost. The number of input harmonic pairs used in the estimator is denoted by the symbol K. In the case of VSD, a possible input harmonic vector for the first iteration can be

$$I_{\text{input}} = [\, I_5, I_5^*, I_7, I_7^*, I_{11}, I_{11}^* \,]^T. \tag{10}$$

In this case, the estimator uses three input harmonic pairs, $K = 3$. The input vector is arranged according to the magnitude size in descending order. After the evaluation process, which is described in the next sub-sections, the smallest harmonic and its complex conjugate can be removed in the next iteration, leaving only two input harmonic pairs, $K = 2$. The iteration process keeps reducing the number of input harmonic pairs until the estimation error just satisfies the accuracy requirement.

B. Matrix Equation

Once all linearly independent constraints have been identified, the matrix equation can be expressed as

$$AI_{\text{DFT}} = b = \mathbf{0}, \tag{11}$$

where the matrix A contains complex exponential coefficients. The Fourier series coefficients vector, I_{DFT} contains harmonics I_k. The vector b represents a constant zero vector.

To solve for the estimator, the matrix A is constructed to have the dimension of R rows by $R + 2K$ columns. The number of rows R reflects all usable constraints describing the waveform, while the number of columns $R+2K$ reflects R constraints and the number of input harmonics $2K$, described in the last section. The I_{DFT} can be partitioned into sub-blocks

$$I_{\text{DFT}} = [\, I_{\text{goal}} \,|\, I_{\text{others}} \,|\, I_{\text{input}} \,]^T, \tag{12}$$

where the variable I_{goal} is the estimated harmonic, specifically the fundamental harmonic, I_1. The vector I_{input} consists of the input harmonic pairs as shown in (10). The vector I_{others} is comprised of other non-zero harmonics. The columns of matrix A have to be rearranged in the similar order

$$A = [\, A_{\text{goal}} \,|\, A_{\text{others}} \,|\, A_{\text{input}} \,], \tag{13}$$

where the matrix A_{goal} is a column vector of size R-by-1, containing coefficients associated with the goal harmonic, specifically the fundamental harmonic I_1 in this case. The matrix A_{input} contains all coefficients corresponding to the input harmonics in I_{input} and has a dimension of R-by-$2K$.

After the matrix A and the DFT coefficient vector I_{DFT} have been rearranged in a desired format, the next section shows the manipulation of the matrix A to obtain the estimator. Specifically, the manipulation will modify the matrix A such that it contains a row relating I_{goal}, i.e. I_1, to a small subset of input harmonics I_{input} with all other harmonics in this row having zero coefficients.

C. Reduced Row Echelon Form

Once the system of equations has been set up in the matrix format, the next step is to compute the functional relationship between different harmonics. The algorithm uses a Gaussian elimination method to reduce the matrix A into

a reduced row echelon form (RREF), A_{RREF}. After the Gaussian elimination process has been performed, the matrix equation in (11) can be expressed in block matrices as

$$A_{\mathrm{RREF}} I_{\mathrm{DFT}} = \left[\begin{array}{c|c|c} 1 & \mathbf{0} & C_{\mathrm{goal}} \\ \hline \mathbf{0} & \mathbf{I} & C_{\mathrm{others}} \end{array}\right] \left[\begin{array}{c} I_{\mathrm{goal}} \\ I_{\mathrm{others}} \\ I_{\mathrm{input}} \end{array}\right] = \mathbf{0}. \tag{14}$$

By rearranging the terms in (14), the estimator can be described by a linear equation with complex coefficients,

$$I_{\mathrm{goal}} = -C_{\mathrm{goal}} I_{\mathrm{input}}. \tag{15}$$

This estimator computes I_{goal} from a input harmonics I_{input}. This candidate estimator must be verified that it can compute the fundamental harmonic with a reasonable error.

D. Estimator Evaluation

After the estimator has been computed, the estimator is evaluated by performing the estimation of the fundamental harmonic using the actual test current. The performance is measured by the estimation error, which is defined as

$$\text{estimation error}\,(\%) = |I_1 - \widehat{I}_1|/|I_1| \times 100, \tag{16}$$

where the variable I_1 is the measured fundamental harmonic, and the variable $\widehat{I}_1$ is the estimated fundamental harmonic computed by the estimator.

Because the estimator in (15) is computed for a specific number of samples N and a specific set of input harmonics, I_{input}, the estimator may not work well for other sampling rates. The band-limited signal sampled at the sampling frequency above the Nyquist rate should contain all information within the data. If the estimator predicts the fundamental harmonic accurately for a given sampling rate, the estimators derived for higher sampling rates should predict accurately as well because more constraints can be listed in the system of linear equations. The band-limited property should be more accurate as the sampling frequency becomes higher. The zero harmonics approximation in (9) should also be more accurate. The estimator should accurately predict the fundamental current harmonic over a range of N_{samp} samples per cycle. Fig. 4 shows examples of the estimator evaluation for the VSD.

In this example, the test current is shown in Fig. 1. In the first iteration, the estimators were derived using three harmonic pairs $K = 3$ as listed in (10) and different sample numbers N_{samp}. The estimation errors for $K = 3$ cases are shown in Fig. 4c. The errors are below 0.4 percent, indicating that the fundamental harmonic of the VSD can be estimated accurately using three harmonic pairs $K = 3$ indicated in (10).

In the next iteration, the input harmonics are reduced to two harmonic pairs the fifth, seventh, and their complex conjugates, $K = 2$. The procedures are reiterated to obtain the estimator for $K = 2$ and different sample points N_{samp}. The estimation errors are shown in Fig. 4b. The errors are below 2.5 percent across a wide range of sample points N_{samp}. As a result, the VSD estimator can use only two harmonic pairs $K = 2$ to estimate the fundamental harmonic with a reasonable error.

To examine if the number of input harmonics I_{input} can be further reduced, the final iteration was done with $K = 1$, using only the fifth harmonic and its complex conjugate. The estimation errors are shown as a function of sample points N_{samp} in Fig. 4a. The result demonstrates the estimation error above 10 percent for many sample points. This result implies that the estimators will not perform consistently across different sample rates. Therefore, the VSD estimator

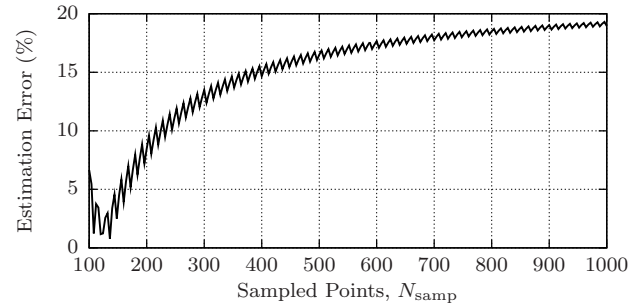

(a) $K = 1$

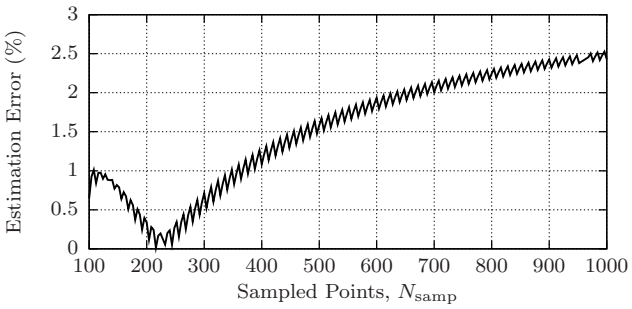

(b) $K = 2$

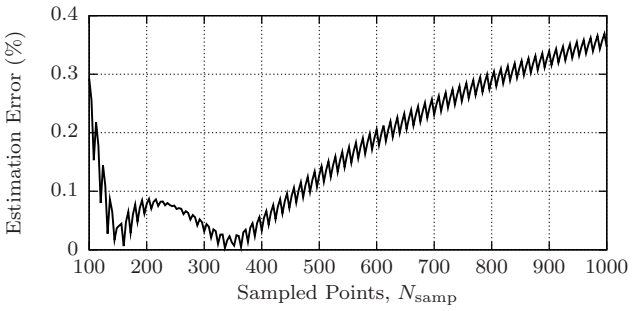

(c) $K = 3$

Fig. 4. Example of estimation errors as a function of sample points N_{samp} and input harmonic pairs K. Simulated VSD current waveform was used in these three cases.

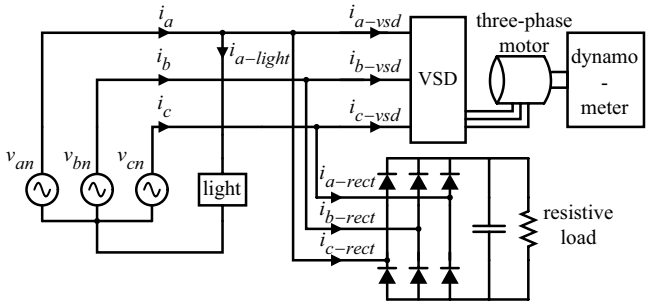

Fig. 5. The experimental setup for extracting the VSD and three-phase rectifier power from the incandescent light bulb

derived using the proposed procedures should use at least two harmonic pairs $K = 2$ to accurately predict the fundamental harmonic.

This section has demonstrated the iterative procedures to derive the estimators based on the five waveform features by using the VSD load as an example. The input harmonics I_{input} are chosen according to their availability and magnitude. The estimator is computed using a simple Gaussian elimination algorithm. Then the performance of the estimator is tested for consistency by measuring the estimation error against the test current. The procedures are repeated with the reduced number of input harmonics by removing the harmonic with the smallest magnitude. The iteration is finished when the estimation error exceeds the requirement. The proposed method provides a guideline to compute the estimator in a linear form. A user has the freedom to select the input harmonics for I_{input}. The evaluation process will verify whether an accurate estimator can be derived using the selected harmonics.

Because the estimator is computed for different sample points N_{samp}, the computational error from the floating point arithmetic can mask the potential of the algorithm as the number of sample points N_{samp} increases. To avoid the floating-point error problem, the proposed method uses a cyclotomic field to represent the complex coefficients in the matrix A as described in [13]. The computation is done using the GP mathematical language [14].

IV. Experimental Results and Discussions

This section demonstrates the ability of the estimator to extract variable power loads such as VSDs, computers, and light dimmers from a fixed linear load.

The first test involves extracting a VSD and three-phase rectifier power from a 50-W incandescent light bulb. The experimental setup is shown in Fig. 5. The VSD estimator is given by

$$\begin{aligned}\widehat{I}_1^{\text{vsd}} =& (1.358 - 0.102j)I_5 + (-0.903 - 0.102j)I_5^* \\ &+ (0.731 - 0.082j)I_7 + (-0.547 - 0.082j)I_7^*.\end{aligned} \quad (17)$$

The fundamental real power of the three-phase load can be computed by

$$P_{3-\text{ph}} = \frac{1}{2}\mathcal{R}\text{e}(V_{an}I_{1,a}^* + V_bI_{1,b}^* + V_{cn}I_{1,c}^*), \quad (18)$$

and the fundamental reactive power can be computed by

$$Q_{3-\text{ph}} = \frac{1}{2}\mathcal{I}\text{m}(V_{an}I_{1,a}^* + V_{bn}I_{1,b}^* + V_{cn}I_{1,c}^*). \quad (19)$$

The real and reactive powers of the single phase load are defined as

$$P = \frac{1}{2}\mathcal{R}\text{e}(V_1I_1^*) \text{ and } Q = \frac{1}{2}\mathcal{I}\text{m}(V_1I_1^*), \quad (20)$$

respectively.

Fig. 6 depicts the extraction of real power of the VSD and a three-phase rectifier load from a 50-W incandescent light. The extraction result resembles the operation of the VSD and the three-phase rectifier. The residual power clearly shows a constant power consumption of the incandescent light.

In the case of a computer, the estimator is derived using the zero-current regions shown in Fig. 2. The computer is connected in parallel with a 100-W light bulb. The computer is expected to consume the current during the window specified as a function of electrical angle specified in radians,

$$i[n] = 0 \text{ for } \frac{2\pi n}{N} \in \left[0, \frac{\pi}{3}\right] \cup \left[\frac{2\pi}{3}, \frac{4\pi}{3}\right] \cup \left[\frac{5\pi}{3}, 2\pi\right). \quad (21)$$

The computer estimator is given by

$$\begin{aligned}\widehat{I}_1^{\text{comp}} =& (-0.744 - 1.214j)I_3 + (-0.324 - 0.636j)I_3^* \\ &+ (0.458 - 0.898j)I_5 + (-0.673 - 0.530j)I_5^* \\ &+ (0.326 - 0.026j)I_7 + (-0.145 + 0.200j)I_7^*.\end{aligned} \quad (22)$$

Experimental results in Fig.7 show that the power consumption of the computer can be cleanly extracted from the aggregate measurements. The residual power consumption clearly shows the operations of the incandescent light bulb with a constant power consumption.

In the last experiment, the estimator is derived to extract the power consumption of the TRIAC-based light dimmer from a fixed 250-W light bulb. The dimmer adjusts the brightness and power consumption by varying the firing angle of the TRIAC to chop off the sinusoidal input voltage feeding the incandescent light bulb as shown in Fig. 3 for example. The estimator for the light dimmer has been developed similar to (22). The estimator uses an approximated current waveform without the initial current at the beginning of the cycle. This approximation allows the five waveform features to be recognized more easily. In the case of a light dimmer, four harmonic pairs are used to estimate the fundamental harmonic currents. Specifically, the estimator uses the third, fifth, seventh, and ninth harmonics. The detail of the estimator for the light dimmer are described in [13]. Experimental results are shown in Figs. 8.

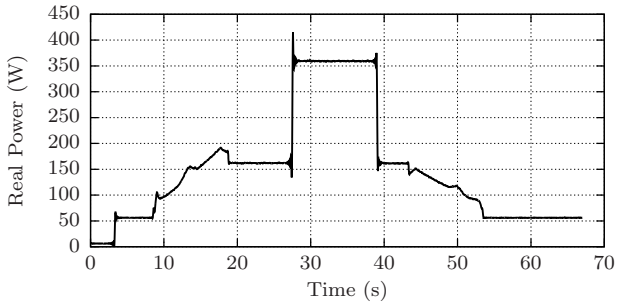

(a) Aggregate real power consumption of the VSD, the rectifier, and the incandescent light

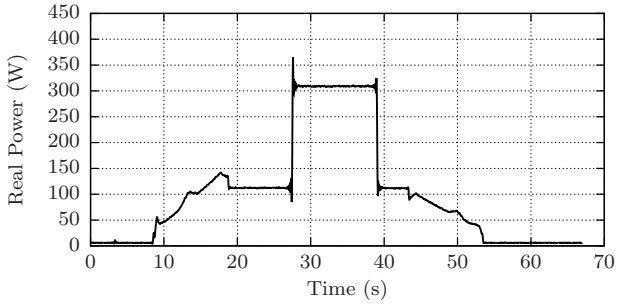

(b) Estimated real power consumption of the VSD and the rectifier

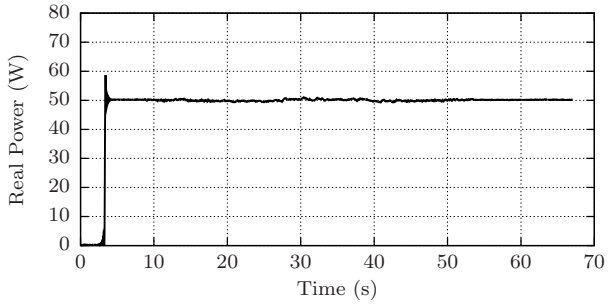

(c) Estimated real power consumption of the incandescent light

Fig. 6. Demonstration the waveform-based estimator extracting the VSD and three-phase rectifier power consumption from an incandescent light. The light bulb turns on at the time $t = 4$ seconds and never turns off. The VSD starts up at the time $t = 8$ seconds and reaches the steady state at the time $t = 18$ seconds. The fixed-load, three-phase rectifier then turns on at the time $t = 27$ seconds and turned off at the time $t = 39$ seconds. The VSD starts to ramp down the power at the time $t = 43$ seconds and completely stops at the time $t = 53$ seconds. The total real power of the VSD, three-phase rectifier, and the incandescent light is shown in (a). The estimated real power consumed by the VSD and three-phase rectifier is shown in (b). The estimated real power consumed by the incandescent light is shown in (c).

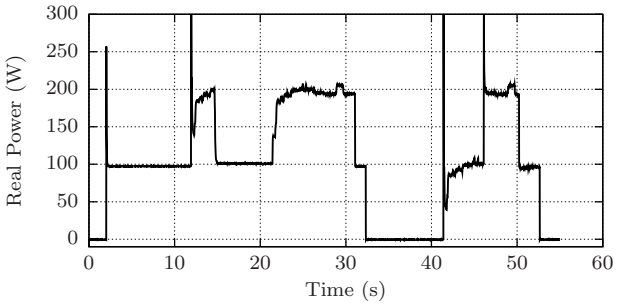

(a) Aggregate real power consumption of the computer and the incandescent light

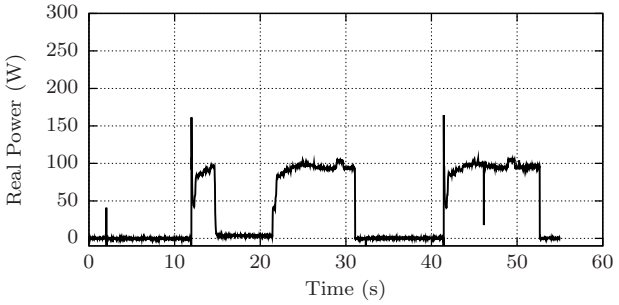

(b) Estimated real power consumption of the computer

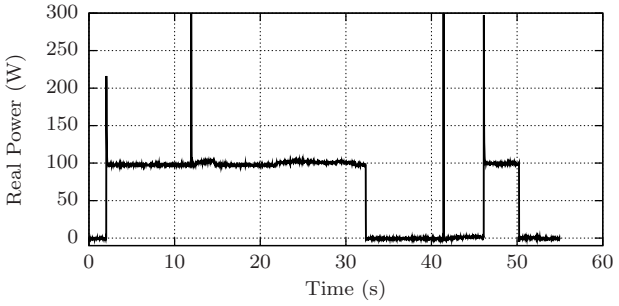

(c) Estimated real power consumption of the incandescent light

Fig. 7. Demonstration the waveform-based estimator extracting a computer's power consumption from an incandescent light. The light turns on at $t = 2$ seconds and turns off at $t = 32$ seconds. The computer was turned on at $t = 12$ seconds and turned off at $t = 15$ seconds. The computer was turned on again at $t = 22$ seconds and turned off at $t = 31$ seconds. Finally, the computer was turned on at $t = 42$ seconds and turned off at $t = 53$ seconds. During the last computer activity, the light was turned on at $t = 46$ seconds and turned off at $t = 50$ seconds. The aggregate real power consumption of the computer and the incandescent light is shown in (a). The estimated real power consumed by the computer is shown in (b). The estimated real power consumed by the incandescent light is shown in (c).

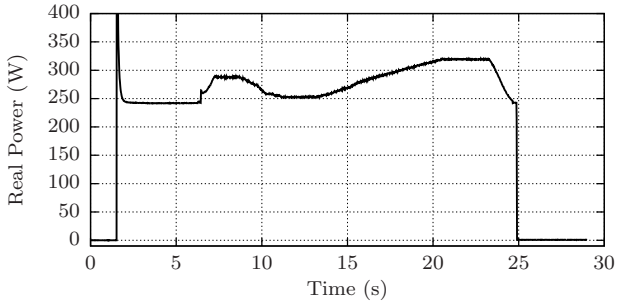

(a) Aggregate real power consumption of the light dimmer and the incandescent light

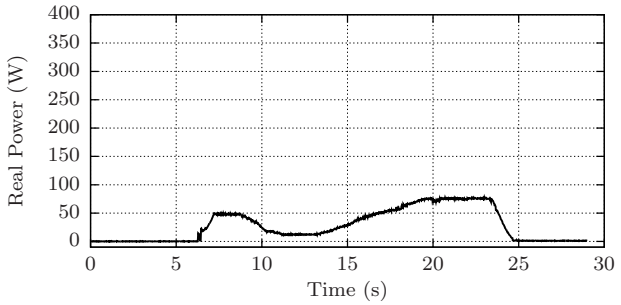

(b) Estimated real power consumption of the light dimmer

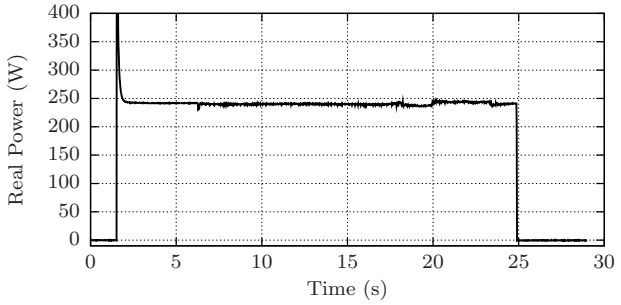

(c) Estimated real power consumption of the incandescent light

Fig. 8. Demonstration the waveform-based estimator extracting a light dimmer's power consumption from an incandescent light. The real power consumption of both the incandescent light and the light dimmer is shown in (a). The 250-W light was turned on at $t = 2$ seconds. Next, the light dimmer was turned on at $t = 7$ seconds. The power consumption of the dimmer was varied continuously. Finally, both the incandescent light and the light dimmer were turned off at $t = 25$ seconds. The estimated real power consumed by the light dimmer is shown in (b). The estimated real power consumed by the incandescent light bulb is shown in (c).

The experimental results demonstrate that the estimator can track the real and reactive power consumption of the light dimmer reasonably well. The incandescent light consumes mostly the real power as expected. The reactive power is mostly consumed by the light dimmer. The result shows that the estimator can track the reactive power of the light dimmer accurately.

Three experimental results have demonstrated the ability of the waveform-based estimator to resolve and track the real and reactive power of the variable power loads. The four-step procedure is described in detail how to derive the estimator from the five-waveform features. The iterative process systematically reduces the number of input harmonics used for estimation to the smallest number when possible. The estimator is computed off-line and the results are the coefficients for different input harmonics. The actual estimation only involves only few multiplications and additions. The actual computation can be performed in real time.

V. Conclusion

This paper has shown the capability of the waveform-based estimator to extract the power consumption of variable power loads from fixed power loads. The proposed method provides a systematic process to derive an estimator for any variable power load with structural features in the current waveforms without a full analysis of internal circuits. The method can possibly be applied for other variable power loads with unique waveform features. The ability to disaggregate the power consumption of each load could supplement the "smart" metering device in the area of diagnostic monitoring, where potential health issues of electrical loads can be monitored and detected in an early stage. The early warning can potentially save a major repair cost and minimize the operational downtime.

References

[1] S. B. Leeb, S. R. Shaw, and J. L. Kirtley, "Transient event detection in spectral envelope estimates for nonintrusive load monitoring," *IEEE Trans. Power Del.*, vol. 10, no. 3, pp. 1200–1210, Jul 1995.

[2] K. D. Lee, "Electric load information system based on non-intrusive power monitoring," Ph.d. Thesis, Mass. Inst. of Tech., Jun 2003.

[3] R. W. Cox, P. Bennett, D. McKay, J. Paris, and S. B. Leeb, "Using the non-intrusive load monitor for shipboard supervisory control," in *IEEE Electric Ship Technologies Symposium*, Arlington, VA, May 2007.

[4] S. R. Shaw and C. Laughman, "A kalman-filter spectral envelope preprocessor," *IEEE Trans. Instrum. Meas.*, vol. 56, no. 5, pp. 2010–2017, Oct 2007.

[5] S. R. Shaw, S. B. Leeb, L. K. Norford, and R. W. Cox, "Nonintrusive load monitoring and diagnostics in power systems," *IEEE Trans. Instrum. Meas.*, vol. 57, no. 7, pp. 1445–1454, Jul 2008.

[6] K. D. Lee, S. B. Leeb, L. K. Norford, P. R. Armstrong, J. Holloway, and S. R. Shaw, "Estimation of variable-speed-drive power consumption from harmonic content," *IEEE Trans. Energy Convers.*, vol. 20, no. 3, pp. 566–574, Sep 2005.

[7] W. Wichakool, A. Avestruz, R. W. Cox, and S. B. Leeb, "Modeling and estimating current harmonics of variable electronic loads," *IEEE Trans. Power Electron.*, vol. 24, no. 12, pp. 2803–2811, Dec 2009.

[8] L. C. Washington, *Introduction to Cyclotomic Fields*, 2nd ed. Springer, 1997.

[9] Z. Remscrim, "The theory and application of non-intrusive load monitoring," Master's thesis, MIT, 2010.

[10] J. H. W. Lenstra, "Euclid's algorithm in cyclotomic fields," *Journal of the London Mathematical Society*, vol. 2, no. 10, pp. 457–465, 1975.

[11] J. M. Masley and H. L. Montgomery, "Cyclotomic fields with unique factorization," *Journal fr die Reine und Angewandte Mathematik*, no. 286-287, pp. 248–256, 1976.

[12] A. V. Oppenheim, R. W. Schafer, and J. R. Buck, *Discrete-time Signal Processing*, 2nd ed. Prentice-Hall, 1999.

[13] W. Wichakool, "Advanced nonintrusive load monitoring system," Ph.d. Thesis, Mass. Inst. of Tech., Feb 2011.

[14] K. Belabas. (2010) PARI/GP development headquarters. [Online]. Available: http://pari.math.u-bordeaux.fr/